

LIDARS

https://doi.org/10.1070/QEL16247

Potentialities of laser systems for remote sensing of the atmosphere at a wide variability of optical and physical characteristics: dimensionless-parametric modelling

R.R. Agishev

Abstract. **Within the framework of generalisation of different approaches to the modelling of atmospheric lidars, the methodology capabilities for dimensionless-parametric analysis are expanded. The developed approach simplifies the analysis of the signal-to-noise ratio and potential capabilities of existing and newly developed monitoring systems with a wide variability of atmospheric and optical conditions and a great variety of modern lidars. Its applicability to the problems of remote atmospheric sensing, environmental monitoring and lidar navigation in providing the eye safety, noise immunity and reliability is discussed.**

Keywords: *laser remote sensing, lidar, atmosphere, optical-physical parameters, signal-to-noise ratio, operation range, eye safety, measurement accuracy, noise immunity.*

1. Introduction

In studies of the atmosphere state, a special place is occupied by laser methods of noncontact monitoring which provide a possibility of retrieving data with a high operational speed on large spatial scales, as well as of identifying the dynamics of their changes. Lidar methods of remote sensing that have been comparatively long since proposed [1–4] are based on scattering and absorption of laser radiation by the components under study. Over the past decade, hundreds of lidar systems, strongly different in their design and practical implementation, have appeared, which defines a multitude of parameters of the transmitting and receiving tracts, accessible detection ranges, range of action, etc.

Modern trends are such that system designers are gradually moving away from extensive approaches. As a promising class of sensing systems, microlidars built on the basis of laser diodes [5, 6], eye-safe lidars [7–9], and modulated cw lidars [10, 11] as an alternative to pulsed lidars, are successfully implemented. Another trend is the employment of multiwavelength lidars [12, 13] capable of sensing a medium in a wide spectral range using the effects of elastic and Raman scattering and absorption. In lidar receivers operating both in the analogue regime and in the regime of photon counting [14–18], high-speed photodetectors [9, 17–20] and receiving modules on their basis, with in-built blocks for amplification, digital processing, and control [19, 20], are used.

R.R. Agishev Kazan State Power Engineering University, Krasnosel'skaya ul. 51, 420066 Kazan, Russia, e-mail: ravil_agishev@mail.ru

Received 5 November 2016; revision received 9 January 2017
Kvantovaya Elektronika **47** (2) 140–152 (2017)
Translated by M.A. Monastyrskiy

Traditional approaches to the analysis of the interrelations between the sensing echo-signals, external background, and internal noises have been long ago worked out. Detailed descriptions are based on the use of rigorous models of photodetectors [21–25], which require consideration of a significant number of specific parameters of different photodetectors. At the same time, using the mentioned detailed and deeply justified approaches, the reduced-to-the-input signal-to-noise ratio ρ for a generalised system of direct photodetection, with internal amplification in the presence of internal and external noises, can be presented in the compact form [16, 18, 26, 27]:

$$\rho = \frac{\sqrt{N}P_\mathrm{s}}{\sqrt{P_\mathrm{q}(P_\mathrm{s}+P_\mathrm{b})+P_\mathrm{n}^2}}, \tag{1}$$

where P_s, P_q, P_n, and P_b are the powers of received signal, quantum, internal and background noises, respectively; and N is the number of accumulation cycles.

The signal-to-noise ratio is a traditional criterion of the lidar instrument efficiency, which is most frequently used in practice. The signal-to-noise criterion has integral nature since it involves the parameters of the lidar instrument, atmospheric object under investigation, propagation medium and external background radiation. The convenience of the signal-to-noise criterion is that it takes into account the result of a combined effect of many factors.

However, the integrity of this criterion is simultaneously its weak point, because sometimes it is very difficult to separate different factors and to assess individually their impact in order to make easier the task of a developer and user. It is quite obvious that a comparison of efficiency of different lidar systems and their potential capabilities is correct only if the experimental conditions, which include, apart from the instrumental characteristics, also optical and physical parameters of the investigated medium and external background radiation, range factor, etc., are similar. In the absence of critical evaluation of the impact of different factors separately, it is very difficult to evaluate the efficiency of lidar subsystems and the measurement instrument as a whole [16, 28–30]. Therefore, when formulating the criteria of a comprehensive assessment of the capabilities of a particular lidar instrument, it is helpful to make them versatile and dimensionless in order to ensure their applicability in different operation conditions and different applications of atmospheric monitoring.

In traditional evaluation of potential capabilities and comparison of lidar systems in terms of the diversity of objectives and tasks of monitoring and encountered atmospheric-optical situations, various assumptions are often accepted to simplify the analysis [31–33]. These assumptions, as a rule,

are based on the commonly used interrelations between the receiving tract characteristics and proceed from significant excess of a particular noise over the others. As a result, the reliability of estimates and the quality of comparisons turn out not high due to the limited set of situations in which they can be actually applied. Herewith, physical meaning is often lost behind the formal algorithms and the 'games' with their analytical and graphical representations.

Another limitation of traditional approaches to the analysis of potential capabilities of the laser remote sensing systems is a somewhat contemplative account for the impact of the background noise, dark noise and other lidar receiver noises [14, 18, 26] – only as the sources of excess noises. This often overshadows the characteristics of a sensed medium, the lidar instrument parameters, etc. Our approach allows us to overcome these limitations.

Finally, in recent years, the international networks for atmospheric research have been established, which unite research teams in partner universities, such as EARLINET-1 and EARLINET-2 (European Aerosol Research Lidar Network to Establish an Aerosol Climatology), ACTRIS-1 and ACTRIS-2 (Aerosols, Clouds & Trace Gases Research Infra-Structure), CLOUDNET, SPALINET and others. Joint workshops on remote sensing of atmospheric parameters are held on a regular basis, the results are analysed and published in close collaboration [19, 20, 34]. The networks include many laboratories and working groups in different countries, most of them employing lidars which are not produced in series. The instruments vary in structure, design and configuration, but at the same time, it is obvious that, in the frame of these networks, it is necessary to ensure homogeneity of the results to make possible an adequate comparison of the data obtained at different stations. In this regard, the network participants have repeatedly expressed their wishes regarding the development of efficient methodologies for the lidar potential evaluation, which would allow the comparison of various instruments for atmospheric sensing, from microlidars to systems employing the super-power pulsed lasers.

Below we discuss the problems of selection and generalisation of criteria that can be applied to assess the potential capabilities and efficiency of lidars for a wide range of problems of remote sensing of the atmosphere and environment. These criteria should be convenient as a basis for the methodology of comparison as well as for a justified choice of the instrument for specific applications.

The aim of our work is a further development and extension of the methodology of dimensionless-parametric modelling of the laser remote sensing systems [15–17, 28–30, 35–37] for maximum generalisation of the criteria and simplification of the analysis of potential capabilities of the existing and newly developed systems, and also for enabling comprehensive and efficient comparison of the transceivers of different lidars under the conditions of broad variability of atmospheric optical monitoring situations and wide variety of approaches to the sensing system design and the instrumental base used.

2. Methodology

Our approach is used for the analysis and integrated comparison of the systems for atmospheric sensing and provides generalisation, modification and simplification of traditionally used algorithms aimed at evaluation of the signal-to-noise ratio and the accuracy of measurements along the measuring path. These algorithms are transformed and further processed in such a way that the individual components of the signal-to-noise ratio, which are determined by the 'range' profile of the lidar echo-signal that the system has actually received, and the sources of noises and interferences of different nature, are normalised to the reference signal power. It is assumed that the introduced reference echo-signal is stimulated and received by the transceiver of the same lidar at the reference distance in the process of sensing of a carefully selected reference atmospheric object (the molecular atmosphere has been selected), which is conducted in the presence of the background sky radiation with a reference brightness.

Thus, using a set of simple and physically transparent dimensionless parameters, a problem is formulated to couple and algorithmically combine the most important components of laser sensing, namely, components of the transceiver system, medium under study and ambient background radiation, which jointly determine the lidar potential and its capabilities as a tool for remote monitoring. This approach facilitates the quantitative comparison of the characteristics of different lidars, offering an *a priori* generalised evaluation of their potential capabilities based on input dimensionless parameters. It also makes possible to demonstrate the capabilities and limitations of particular systems, both existing and newly developed ones, providing simple physical meaning and clearness to the results.

The brightness of the sky radiation as a source of background interference is also normalised to the reference brightness of background interference selected as the lower limit of a typical range of sky brightness for mid-latitudes, which is certainly present in the sensitive area of a lidar photodetector.

2.1. Reference medium and range. Reference background brightness

Consider the case of monostatic sensing by means of a backscattering lidar, when the optical emitter and the receiving system are located in close proximity to each other. A spatial change in the optical parameters of the atmosphere along the sensing path is related to the backscattered radiation power by the known expression, which is called the equation of laser sensing, or lidar equation [1–3] and, in the single-shot scattering approximation, has the form

$$P_s(\lambda, R) = {}^1\!/_2 G(R)\xi(\lambda)cE(\lambda)A_D\beta_\pi(\lambda, R)\,T^2(\lambda, R)\,R^{-2}, \quad (2)$$

where

$$T(\lambda, R) = \exp\left[-\int_0^R \alpha(\lambda, r)\,\mathrm{d}r\right]; \quad (3)$$

E is the emitter pulse energy; c is the speed of light; λ is the wavelength; R is the current sensing range; A_D is the receiving lens area; $\beta_\pi = \sigma_\mathrm{v} i_\pi$ is the volumetric backscattering coefficient; σ_v is the volumetric scattering index; i_π is the lidar ratio, or the modulus of the scattering indicatrix vector for the angle π; α is the volumetric attenuation index; ξ is the receiving optical system transmission; $G(R)$ is the lidar geometrical factor characterised by the overlapping integral of the sensing beam and the receiver field of view [$G(R) = 1$] in the case of a full overlap; and T is the transmittance, or the transparency of the atmosphere.

2.1.1. Molecular atmosphere as a reference medium. Reference echo-signal. For evaluation of the potential capabilities of a lidar instrument and correct comparison of the efficiency of engineering solutions used in the development of

various instruments, it is advisable to select a generalised lidar parameter, or a system of lidar parameters, as a criterion for the comparison and evaluation. On the one hand, such a parameter should characterise the measurement system itself. On the other hand, for the benefit of practical application, a properly chosen criterion for the comparison of different lidar instruments should include the parameters of a certain standard scattering object of research and a typical propagation medium. The role of such a versatile test object may be successfully plaid by the molecular atmosphere, the standard parameters of which are generally accepted. For example, it is often assumed that at $\lambda = 0.55$ μm, the volumetric attenuation of the standard molecular atmosphere at normal conditions is $\alpha_0 = 0.0116$ km^{-1}, and the scattering indicatrix of the molecular atmosphere is $i_{\varphi 0} = 3(1 + \cos^2\varphi)/16\pi$ [38, 39], whereas, for the scattering angle $\varphi = \pi$, the indicatrix value is taken equal to $3/8\pi$.

The use of a reference medium has several advantages:

1. Comparison of the lidar echo-signals received from a standardised test object in the absence of atmospheric variability provides a direct and easy comparison of the lidar potentials.

2. Comparison of the lidar echo-signals coming from an arbitrary atmospheric object and normalised to the signals of the reference molecular atmosphere provides a direct estimate of the measurement sensitivity reached by each system.

3. Comparison of the reference echo-signals with the signals conditioned by different atmosphere states along the sensing path (e.g., layers with high aerosol concentration, etc.) allows direct evaluation of the impact of atmospheric attenuation of the signals along the sensing path on the potential capabilities of lidar measurements.

2.1.2. Reference echo-signal of molecular atmosphere and reference range. As the reference signal, we choose the echo-signal $P_{s0}(\lambda, R_0)$ of the backscatter lidar, received at the sensing wavelength λ at a certain reference distance R_0 for the standard conditions of the molecular atmosphere. The reference distance R_0 can be viewed as a natural linear scale, which may or may not be significant for the system under study. Then,

$$P_{s0}(\lambda, R_0) = {}^1/_2 \xi(\lambda)\, cE(\lambda)\, A_D \beta_{\pi 0}(\lambda, R_0)\, T_0^2(\lambda, R_0)\, R_0^{-2}. \qquad (4)$$

The attenuation coefficient of clean atmosphere [26, 27], when the meteorological visibility range S_m exceeds 10 km, can be represented as $\alpha(\lambda) = (\lambda/0.55)^{-q}(3.91/S_m)$, where $q = 0.585\, S_m^{1/3}$; and λ is taken in μm and S_m in km.

Note that the normalisation of the lidar instrument's range R by a reference distance R_0 to the test object allows us to use a dimensionless range factor $r = R/R_0$, which facilitates the comparison of results. The absolute value R_0 may be chosen differently, depending on particular conditions of the lidar application.

2.1.3. Reference sky background brightness. When conducting atmospheric-optical measurements, the reception of echo signals carrying information about the medium properties is performed in the presence of background radiation. In contrast to the laboratory measurements, when, as a rule, it is possible to eliminate background radiation sources or compensate for their effects, the background intensity in the natural atmosphere can be very high, and it turns out much more difficult to rule out the background interference. Background radiation is usually understood as photons incoming to the optical receiver in the form of a stream or as temporally resolvable individual photons that impede the correct reception of echo-signals, are not related in their nature to the echo-signals, and their spectrum lies within the receiver sensitivity bandwidth. By the place of emergence and origin, background radiation is usually attributed to external natural interferences. Protection from background interferences is one of the important tasks in the process of selection of useful information in lidar measurements [14, 27, 32, 38, 39].

Natural illumination conditions under the open sky are determined by three main sources: the Sun which represents a moveable and virtually point-like primary source; the sky, i.e., the atmosphere which scatters the sunlight; the ground coverings which reflect incident light of the Sun and sky. Due to the Sun motion and changes in the state of the atmosphere and ground coverings, the light field generated by these sources continuously changes in time. Therefore, natural illumination of the sky is a complex function of time, having stochastic nature.

The main source of the daytime sky glow in the spectrum region with the wavelengths less than 3 μm is the scattered solar radiation. Evaluating the Sun brightness as $B_{S\lambda} = 2hc^2 \times (\lambda^5\{\exp[hc/(\lambda kT)] - 1\})^{-1}$, it is sometimes accepted that, at a wavelength of 0.5 μm, the colour temperature of the Sun is 6500 K, while its average brightness in the visible range is 2×10^9 cd m^{-2} [2, 21, 40]. Commonly, it is assumed equal to 10^{-5} of the Sun brightness, whereas the day-sky brightness to a large extent depends on the Sun position in the sky and the height of the place of observation above the sea level.

Similarly to the above-introduced reference echo-signal P_{s0} and the reference range R_0, we introduce the reference brightness $B_{0\lambda}$ of the sky background. At mid-latitudes, in the wavelength range 0.3–1.1 μm (from UV to near-IR range), the typical background brightness range of the daytime sky is $B_\lambda = 10^6 - 3\times10^8$ W m^{-2} sr^{-1} m^{-1} [21, 26, 27]. We accept the reference brightness $B_{0\lambda}$ of the sky equal to 10^6 W m^{-2} sr^{-1} m^{-1}, which is approximately 300 times less than the maximum background brightness at mid-latitudes. In this case, we assume the background brightness distribution in wavelengths corresponding to the solar radiation spectrum.

The sky background power recorded at the sensing wavelength λ is only determined by the sky background brightness and the receiving system parameters of a particular lidar. The sky background with the reference brightness $B_{0\lambda}$ selected as a lower limit of the typical brightness range for mid-latitudes generates, on the sensitive area of the photodetector of a particular lidar, a background stream having the power [14, 18, 21]

$$P_{b0}(\lambda) = B_{0\lambda}\xi(\lambda) A_D\, \Omega\, \Delta\lambda(\lambda), \qquad (5)$$

which we call the reference background power. Here Ω is the solid angle of the receiving system's field of view, and $\Delta\lambda$ is the spectral filter bandwidth. This background noise level is present, at least, at the photodetector input, and therefore it must be taken into account, when analysing the lidar potential, as a source of the receiver's excess noises. In turn, the background radiation power of an arbitrary brightness can be represented in the form

$$P_b(\lambda) = \frac{B_\lambda}{B_{\lambda 0}} P_{b0}(\lambda) = b_{rel} P_{b0}(\lambda), \qquad (6)$$

where

$$b_{\text{rel}} = B_\lambda / B_{0\lambda} \tag{7}$$

is the relative sky background brightness.

3. Dimensionless-parametric model of the lidar system as a tool to evaluate the lidar potential and efficiency

Now we perform a normalisation of all components of Eqn (1) with respect to the introduced reference echo-signal of the molecular atmosphere (4) (N is the number of accumulation cycles):

$$\rho = \frac{P_s\sqrt{N}}{\sqrt{P_q(P_s + P_b) + P_n^2}} = \frac{\sqrt{N}P_s/P_{s0}}{\sqrt{(P_q/P_{s0})(P_s/P_{s0} + P_b/P_{s0}) + P_n^2/P_{s0}^2}}. \tag{8}$$

3.1. Normalised echo-signal

From relations (2)–(4) we obtain a power ratio of the echo-signal and the reference signal:

$$P_s(\lambda,\alpha,R)/P_{s0}(\lambda,\alpha_0,R_0) = [\beta_\pi(\lambda,R)/\beta_{\pi0}(\lambda,R_0)] \times [T(\lambda,\alpha,R)/T(\lambda,\alpha_0,R_0)]^2 (R_0/R)^2.$$

The following notations are introduced: $Q = \beta_\pi(\lambda,R)/\beta_{\pi0}(\lambda,R_0) = i_\pi(\lambda,R)\alpha(\lambda,R)[i_{\pi0}(\lambda,R_0)\alpha_0(\lambda,R_0)]^{-1}$ (here $\sigma_v = \alpha$) and $W = T(\lambda,\alpha,R)/T(\lambda,\alpha_0,R_0)$. In many cases, the expression $\beta_\pi(\lambda) = 0.019\alpha^{0.57}(\lambda)$ holds true (α is taken in km^{-1}) [27, 38, 39], especially, in the molecular atmosphere $\beta_{\pi0}(\lambda) = (3/8\pi)\alpha_0(\lambda)$. Let us now combine the parameters Q, W and r into a normalised lidar signal

$$\Pi \equiv P_s/P_{s0} = QW^2r^{-2}, \tag{9}$$

which characterises the relative atmospheric-optical situation (optical 'weather') along the sensing path with regard to the squared range, reduced to the molecular atmosphere state taken as a reference. In the estimates of the variation range Π of the normalised echo-signal for aerosol backscatter lidar in the homogeneous atmosphere, we may assume that $\Pi = [\beta_\pi(R)/\beta_{\pi0}(R_0)]\exp[-2(\alpha R - \alpha_0 R_0)](R_0/R)^2$.

The information about the International visibility scale, giving an idea of the interrelation of the meteorological visibility range S_m with the transparency T and the volumetric attenuation index α of the atmosphere at different observation conditions, is presented in Appendix 1.

3.2. Partial signal-to-noise ratios

We introduce the partial signal-to-noise ratios S_q, S_{b0} and S_n, which are understood as the partial indicators of sensitivity (potential) deterioration of a sensing system, caused by the Schottky noise of the signal and background interference, and also by the internal noise of the photodetector:

$S_q = P_{s0}/P_q$ is the partial power ratio of the reference signal and quantum noise of the detector, reduced to the input;

$S_n = P_{s0}/P_n$ is the partial power ratio of the reference signal and internal noise of the detector; and

$S_{b0} = P_{s0}/P_{b0}$ is the partial power ratio of the reference signal and reference background.

The feasibility of introducing the partial ratios S_q, S_n, S_{b0} and parameter Π is that they allow taking into account various sources of internal and external noises peculiar to a particular system, and to couple these noises to the parameters of the medium being sounded. Thus, the system noises and their impact are considered not by themselves, but in comparison with the reference echo-signal received from an accepted reference distance and formed as a result of sensing of the reference atmosphere by a particular lidar when exposed to the background interference with reference brightness, which is, at least, present at the photodetector input. The analysis is conducted using the transceiver parameters of a lidar system, and is thus 'attached' to a particular instrument for remote atmospheric sensing.

3.3. Degree of excess of lidar receiver noises over quantum noises

Let us perform simple transformations of the signal-to-noise ratio using Eqn (8) with regard to Eqn (7):

$$\rho = \frac{\sqrt{N}P_s/P_{s0}}{\sqrt{(P_q/P_{s0})(P_s/P_{s0} + P_b/P_{s0}) + P_n^2/P_{s0}^2}} = \frac{\Pi\sqrt{N}}{\sqrt{S_q^{-1}(\Pi + b_{\text{rel}}/S_{b0}) + S_n^{-2}}} = \frac{\Pi\sqrt{N}\sqrt{S_q}}{\sqrt{\Pi + S_q/S_n^2 + b_{\text{rel}}/S_{b0}}}.$$

To simplify this expression and take into account the parameters of a particular transceiver system, let us introduce the generalised parameter

$$A = b_{\text{rel}}/S_{b0} + S_qS_n^{-2} \tag{10}$$

as a dimensionless characteristic of the lidar noises in the presence of the background interference, which exceed the quantum noise and are normalised to a virtual reference signal. As a result, we obtain a simple expression for evaluation of the signal-to-noise ratio of a lidar system, reduced to the input:

$$\rho = \frac{\Pi\sqrt{N}\sqrt{S_q}}{\sqrt{\Pi + A}} = \frac{\sqrt{\Pi N S_q}}{\sqrt{1 + A/\Pi}}, \tag{11}$$

which is applicable for any laser sensing instruments.

The obvious advantage of presenting the signal-to-noise ratio in form (11) is that the best sensing accuracy is achieved at large (compared to the parameter A) values of the normalised echo-signal Π (at small ratios A/Π), because in that case the larger signal-to-noise ratios along the path and the limiting lidar sensitivity are implemented. In turn, if $A > \Pi$, the excess system noises significantly exceed the quantum noises, thus lowering the accuracy.

As mentioned in the Introduction, in assessing the potential capabilities of lidar systems to simplify the analysis, it is usually assumed that the receiver sensitivity is limited by the quantum noise, whose power $P_q = 2hcF\Delta f/(\lambda\eta)$ is sometimes regarded as a sort of scale for the assessment of the signal levels, background interference and internal noise, because all of them depend on the wavelength λ, noise factor F, bandwidth Δf and quantum efficiency η of the receiver. By adapting the mentioned approaches to expressions (10) and (11), it is

easy to see that the A-factor we have introduced is zero if we only take into account the quantum noise, while the signal-to-noise ratio ρ in this case is equal to $\sqrt{S_q \Pi}\sqrt{N}$. Obviously, the excess noises, which exceed the quantum noises of a real photodetector, are not taken into account in this case.

For the night-sky brightness taken into account in the estimates as a minimum brightness, and assuming that $b_{rel} = 1$, the A-parameter, which characterises the receiver noise in the presence of background, has an important term:

$$A_0 = S_q/S_n^2 + S_{b0}^{-1}. \tag{12}$$

Then, for the day-sky brightness

$$A = A_0 + (b_{rel} - 1)/S_{b0}. \tag{13}$$

As follows from (12), the dimensionless parameter A_0 corresponds to the quantum noise and internal noise of the receiver, and also to the minimal-level background interference present. This parameter is an original measure of excess noises in the lidar receiver with respect to the signal quantum noises that are unavoidably present. The parameter A_0 that is calculated before the sensing experiments provides quantitative information about the significance of the excess noise impact compared to that of the signal quantum noise for a particular transceiver system under condition that the ambient background brightness is equal to the reference brightness.

In the presence of a real background interference, the intensity of which is b_{rel} times higher than that of the reference one (with $b_{rel} = 1$), the excess noise level is determined by expression (13).

Returning to formula (11) with regard to (13), the signal-to-noise ratio in sensing a medium that we have selected as a reference medium, provided the signal is received within the reference range in the presence of the ambient sky background with a reference brightness with $Q = 1$, $W = 1$, $r = 1$ (i.e. $\Pi = 1$), and $b_{rel} = 1$, appears as

$$\rho = \frac{\sqrt{S_q N \Pi}}{\sqrt{1 + A/\Pi}} = \frac{\sqrt{S_q N}}{\sqrt{1 + A_0}}. \tag{14}$$

3.4. Dimensionless system parameter L_0 as a generalised and versatile characteristic of the lidar potential

Following (14), we introduce the dimensionless system parameter L_0 as the signal-to-noise ratio that is reached in receiving the echo-signal in the reference range when sensing the reference atmosphere without accumulation ($N = 1$) and with the reference brightness of the sky background taken into account:

$$L_0 \equiv \rho(\Pi = 1, b_{rel} = 1, N = 1) = \sqrt{S_q/(1 + A_0)}. \tag{15}$$

Thus, L_0 ensures the possibility of predicting the signal-to-noise ratio being reached in receiving the signal in the reference range. The introduction of the parameter L_0 as an algorithmic set of the partial signal-to-noise ratios of different nature, characterising the system noises peculiar to a particular lidar, allows us to estimate the lidar potential and to compare the capabilities of different measuring systems at the preliminary stage, even before remote measurements.

As noted above, the previously used approaches to the normalisation of lidar signals and noises by quantum or other noises [14–17, 22, 27–30, 35–40] are reasonable when comparing different sources of noises. However, their weak point is a somewhat notional consideration of noises and allegedly independent analysis of the received signal and noises. The introduced partial ratios S_q, S_n and S_b, which appear in the expression for A_0 (12), and the key system parameter L_0, 'binds' the noises to the potential of particular lidar instruments and their capability of sensing the reference medium within the reference range, which makes efficient the estimate of real significance of relevant parameters and convenient the comparison.

Moreover, the introduction of the normalised echo-signal Π, which continually 'tracks' the variability of optical and physical properties of the atmosphere along the sensing path and includes the range factor, enables a justified classification and full account of noise characteristics of a particular lidar system. Indeed, only in the case of a properly conducted comparison with a lidar signal, which is determined by the particular optical weather and range included into the Π parameter, the system noise can be considered, for example, as being acceptably low or too high.

Then the signal-to-noise ratio at the lidar receiver output can be conveniently represented in the form of an expression

$$\rho = \frac{\sqrt{S_q \Pi}\sqrt{N}}{\sqrt{1 + [A_0 + (b_{rel} - 1)/S_{b0}]\Pi^{-1}}} = L_0 \Pi \sqrt{N} \frac{\sqrt{1 + A_0}}{\sqrt{\Pi + A_0 + (b_{rel} - 1)/S_{b0}}}, \tag{16}$$

which, in dimensionless form, allows one to easily trace which factors and in what way they affect the resulting signal-to-noise ratio in sensing of an arbitrary atmospheric object, and to compare it with the reference signal-to-noise ratio characterised by L_0, i.e. the first factor in Eqn (16).

General considerations allow for a conclusion that the lower the receiver noises and background interference, the higher the measurement accuracy. However, in particular, it is seen from (16) that the excess system noises determined by the dimensionless parameters A_0 and $(b_{rel} - 1)/S_{b0}$ affect the signal-to-noise ratio, sensitivity and lidar operation range, along with optical and physical characteristics of the sounded object, which define the normalised echo-signal Π. Their significance may be low or, on the contrary, high, depending on the optical state of the weather along the monitoring path. This represents the essential difference of the results obtained from the often-used simplifying estimates, in which the impact of the sounded object properties turns out disguised by the accepted assumptions, which significantly narrow the set of possible atmospheric-optical media and situations.

Figure 1 shows the introduced generalised system parameter L_0 as a function of the excess noise factor A_0 that is determined by only taking into account the reference background level (i.e. at $b_{rel} = 1$) for different values of S_q. It is seen that the photodetectors with a low level of excess noises ($A_0 < 0.5$) does not virtually affect the system potential, which is only determined by a ratio of the reference signal to quantum noises, because, according to (15), in that case $L_0 \approx \sqrt{S_q}$.

In contrast, the 'noisy' receivers ($A_0 \gg 1$) can by many times diminish the lidar potential. We should incidentally note that Eqn (16) clearly shows that the ambient back-

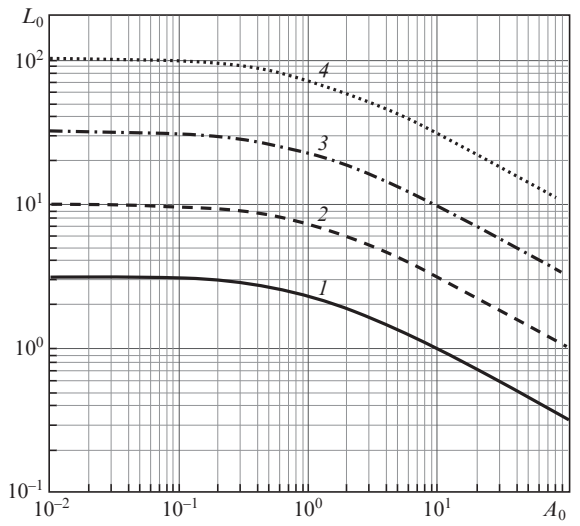

Figure 1. Dependences $L_0(A_0)$ at S_q = (*1*) 10, (*2*) 10^2, (*3*) 10^3 and (*4*) 10^4.

ground interference is not so noticeable when using the noisy photodetectors; however, in any case, the significance of its contribution is comparable with the contribution of the dimensionless parameter Π of the echo-signal. The impact of a real background interference (at $b_{rel} \gg 1$), which can substantially impair the measurement accuracy, is discussed below.

3.5. Impact of excess noises on the signal-to-noise ratio

Now let us turn back to the dimensionless parameterisation of the signal-to-noise ratio (11). The denominator in Eqn (11) characterises the deterioration of the measurement accuracy due to the excess noises of the receiver, which exceed the quantum noises caused by the dark current and also by the presence of background radiation in the sensitive area of the lidar photodetector, which is mostly caused by the scattered solar radiation. We call this value the dimensionless factor Φ_{ex} of reducing the signal-to-noise ratio by excess noises:

$$\Phi_{ex} = \left(\frac{\Pi}{\Pi + A}\right)^{1/2} = \left[\frac{\Pi}{\Pi + A_0 + (b_{rel} - 1)/S_{b0}}\right]^{1/2}$$

$$= \left[1 + \frac{A_0 + (b_{rel} - 1)/S_{b0}}{\Pi}\right]^{-1/2}. \qquad (17)$$

The limits within which the background factor may degrade the signal-to-noise ratio and the distance measurement accuracy are shown in Fig. 2 in the form of the dependences of Φ_{ex} on the ratio

$$\frac{P_b}{P_{s0}} = \frac{A_0 + (b_{rel} - 1)/S_{b0}}{\Pi}$$

for various optical-physical sensing conditions and noise properties of photodetectors. It is clear from Fig. 2 that the significance and impact of the degree of the receiver's internal noise and background noise are not absolute, but depend on the optical-physical properties of the sounded object, which, along with the range factor, determine the Π-value. Indeed,

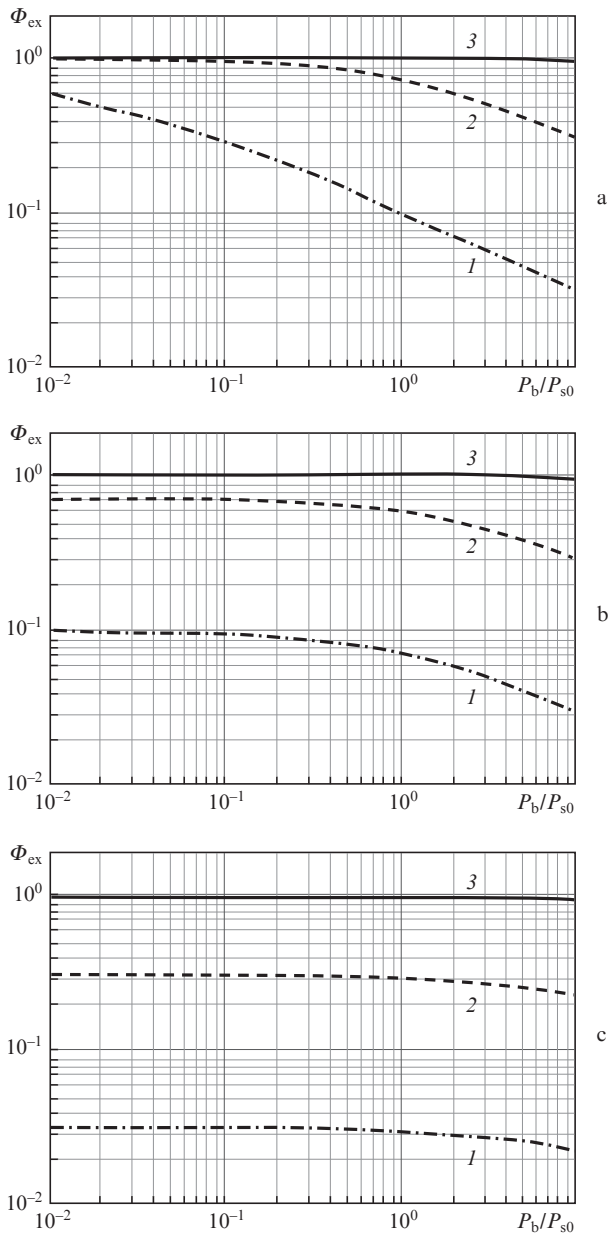

Figure 2. Excess noise factor Φ_{ex} as a function of the ratio P_b/P_{s0} at Π = (*1*) 10^{-2}, (*2*) 1 and (*3*) 10^2, and A_0 = (a) 10^{-2}, (b) 1 and (c) 10.

at $\Pi \gg 1$ the impact of excess noises of the detector and background noises is almost negligible [curves (*3*)]. With decreasing Π, the background noise impact increases; therefore, comparing the dependences for $A_0 \ll 1$ (Fig. 2a) and $A_0 \gg 1$ (Fig. 2c), it can be easily seen that the background effect is much stronger in the case of low-noise photodetectors: the excess noise factor Φ_{ex} causes a relatively sharp decrease in the resulting signal-to-noise ratio even at a relatively low level of background noise. The noisy detectors are only influenced by a sufficiently intense background ($P_b/P_{s0} > 1$).

Note that the night-time (Φ_n) and the day-time (Φ_d) components defined by the parameters A_0 and A, and also by the normalised signal Π, can be distinguished in the excess noise factor Φ_{ex}:

$$\Phi_{ex} = \Phi_n \Phi_d, \quad \Phi_n = \frac{\sqrt{\Pi}}{\sqrt{\Pi + A_0}}, \quad \Phi_d = \frac{\sqrt{\Pi + A_0}}{\sqrt{\Pi + A}}.$$

3.6. Evaluation of the signal-to-noise ratio in recording the signals in photon-counting mode

During the energy reception, the signal at the photodetector output, depending on the intensity of the received flux of photons, may represent either a sequence of pulses that are superimposed to each other, or a 'rare' sequence of pulses that are resolvable, not superimposed to each other, and easy to count. In the first case, the average density of the pulsed flux $\bar{\gamma}$ defined by the number of pulses per unit time $\bar{n}$, which are recorded for the time equal to the temporal resolution τ_{res} of the photodetector, is large: $\bar{\gamma} = \bar{n}\tau_{\text{res}} \gg 1$, where $\tau_{\text{res}} \approx \Delta f^{-1}$. This regime, in which the optical signal envelope is reproduced, is called an analogue, or current, regime. The estimates of the signal-to-noise ratio in form (1), (8) and associated estimates presume such recording regime of the received backscattered signals.

When receiving weak signals, the pulsed flux density is low ($\bar{\gamma} \ll 1$), and the lidar signal envelope cannot be reproduced. The photodetector is capable of capturing single photoelectrons, i.e. of operating in photon counting mode, which is called discrete mode. Input signals are counted against the background of internal and external noises in accordance with the number n of single-electron pulses during the measurement time Δt. By using the amplifier and discriminator, they are transformed into a sequence of standard pulses, while their number is recorded by the counter.

It is accepted that the number n_{s} of photons in the signal recorded by a lidar system, the number n_{b} of photons in the ambient background, and the number n_{d} of dark pulses are described by the Poisson statistics of random processes [14, 21, 27]. Since these processes have equal mathematical expectations M and variances σ^2 ($M = \sigma^2$), their values for n_{s}, n_{b} and n_{d} for the observation time Δt are determined by the expression

$$M_{\text{s}} = \sigma_{\text{s}}^2 = \eta v_{\text{s}} \Delta t, \quad M_{\text{b}} = \sigma_{\text{b}}^2 = \eta v_{\text{b}} \Delta t, \quad M_{\text{d}} = \sigma_{\text{d}}^2 = v_{\text{d}} \Delta t,$$

where v_{s}, v_{b} and v_{d} are the average speeds of counting signal photons, background photons and dark pulses of the photodetector, respectively. In this case, $v_i = P_i/E_0 = P_i\lambda/(hc)$, where i = s, b, d; and E_0 is the quantum energy.

The total number of counts $n_{\text{tot}} = n_{\text{s}} + n_{\text{b}} + n_{\text{d}}$ for the observation time Δt is also a random variable. The expressions for the average value of the number of counts and the variance of three independent Poisson processes have the form

$$M_{\text{tot}} = M_{\text{s}} + M_{\text{b}} + M_{\text{d}},$$

$$\sigma_{\text{tot}}^2 = \sigma_{\text{s}}^2 + \sigma_{\text{b}}^2 + \sigma_{\text{d}}^2 = \eta v_{\text{s}} \Delta t + \eta v_{\text{b}} \Delta t + v_{\text{d}} \Delta t.$$

The signal-to-noise ratio ρ calculated as a ratio of the average number M_{s} of the received signal photons to its mean square deviation σ_{tot} from the total number of photons for the observation time Δt can be presented as

$$\rho = \frac{M_s}{\sigma_{\text{tot}}} = \frac{\eta v_{\text{s}} \Delta t}{\sqrt{\eta v_{\text{s}} \Delta t + \eta v_{\text{b}} \Delta t + v_{\text{d}} \Delta t}},$$

or

$$\rho = \frac{\eta v_{\text{s}} \sqrt{\Delta t}}{\sqrt{\eta v_{\text{s}} + \eta v_{\text{b}} + v_{\text{d}}}}. \tag{18}$$

When accumulating the results of N sensing cycles, we have $M_{iN} = NM_i$ (i = s, b, d), $\sigma_{\text{tot}N}^2 = N\sigma_{\text{tot}}^2$ [15, 36] and

$$\rho = \eta v_{\text{s}} \sqrt{N\Delta t} / \sqrt{\eta v_{\text{s}} + \eta v_{\text{b}} + v_{\text{d}}}. \tag{19}$$

In photon-counting mode, the amplitude of each pulse from the photodetector is compared with the discriminator threshold, and only those pulses are counted whose amplitude exceeds the threshold. Due to their statistical nature, the pulses may sometimes follow with a very small interval, and so they become indistinguishable by the discriminator. This leads to a loss of events or to miscalculations caused by the finiteness of time resolution in the recording devices. Therefore, the so-called 'dead time' τ_{dd} is introduced, which, as applied to photon counting, is generally understood as the minimum time interval within which two close events can be considered as two separate events [14, 18, 27].

Two types of the dead time are distinguished: paralysed/extendable dead time and non-paralysed/non-extendable dead time [27, 41]. In the paralysed case, a single photon initiates the dead time 'extendable' by the next photon that arrives during the time τ_{dd}, which reduces the observed count rate of photons

$$v_{\text{ob}} = v_{\text{a}} \exp(-v_{\text{a}} \tau_{\text{dd}}), \tag{20}$$

where v_{a} is the actual rate of photon counting. In the non-paralysed system, the dead time 'initiated' by a single photon is not extended by the next photon, and

$$v_{\text{ob}} = v_{\text{a}}/(1 + v_{\text{a}} \tau_{\text{dd}}). \tag{21}$$

In lidar measurements, the non-paralysed photodetectors are more commonly used, for which the corrected count rate can be easily derived from (21):

$$v_{\text{a}} = v_{\text{ob}}/(1 - v_{\text{ob}} \tau_{\text{dd}}). \tag{22}$$

In this case, expressions (20)–(22) are applicable for relatively small count rates, when $v_{\text{a}}\tau_{\text{dd}} < 1$.

4. Structure of a dimensionless-parametric model of a lidar system and simulation results

4.1. Structural scheme of the dimensionless-parametric model

As follows from (9) and (16), (17), the signal-to-noise ratio reduced to the lidar receiver input, for $N = 1$ can be presented in the dimensionless-parametric form:

$$\rho = \frac{\Pi\sqrt{S_{\text{q}}}}{\sqrt{\Pi + A}} = \Pi \sqrt{\frac{S_{\text{q}}}{1 + A_0}} \sqrt{\frac{1 + A_0}{\Pi + A}} = \Pi L_0 \sqrt{\frac{1 + A_0}{\Pi + A}},$$

or

$$\rho = \sqrt{\Pi S_{\text{q}}} \frac{\sqrt{\Pi}}{\sqrt{\Pi + A}} = \sqrt{\Pi S_{\text{q}}}\, \Phi_{\text{ex}}. \tag{23}$$

The introduction of the normalised lidar signal $\Pi = QW^2r^{-2}$ allows avoiding the necessity of consideration of a multitude of partial cases and their combinations in analytical prediction. Therefore, both forms of expression (23) are pre-

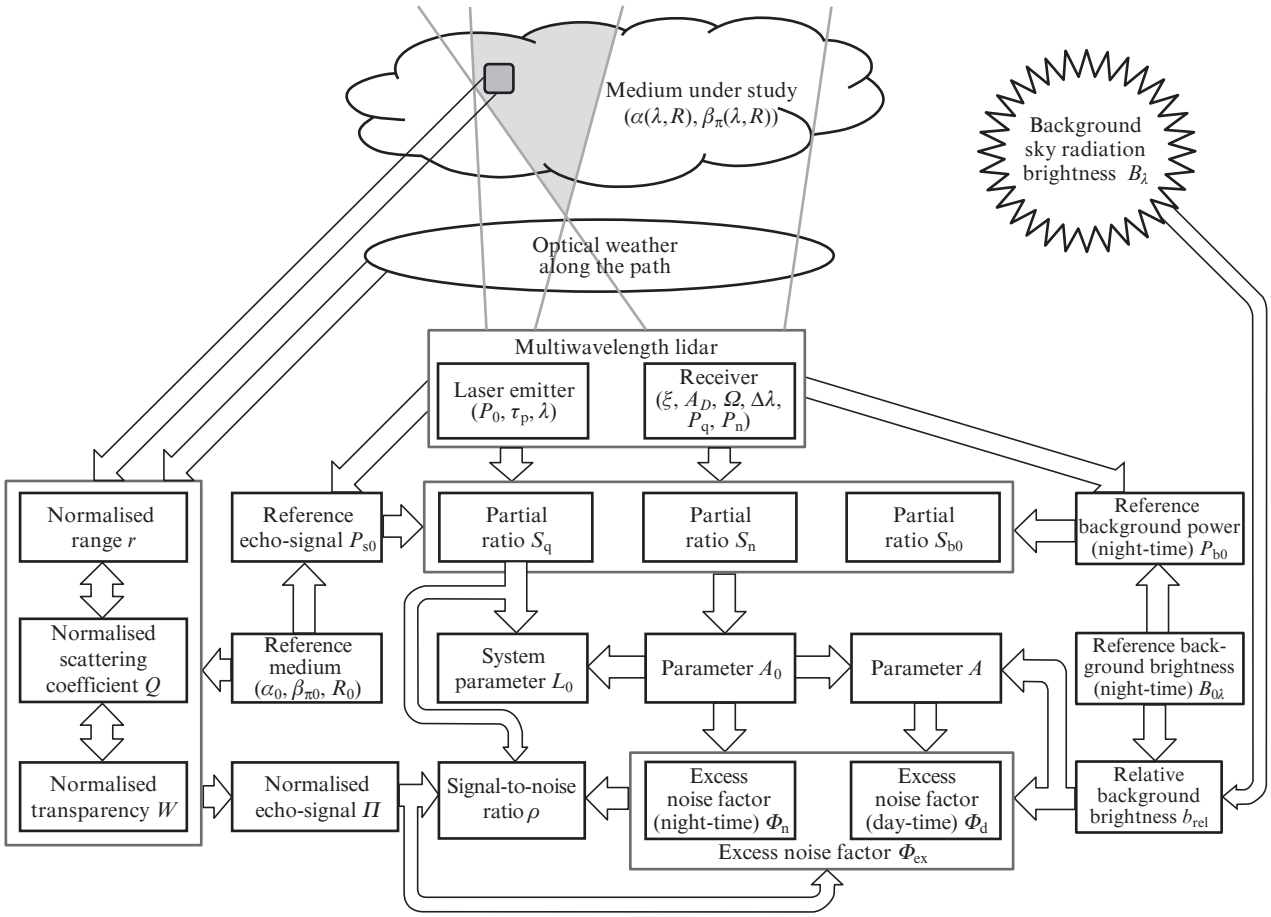

Figure 3. Structure of a dimensionless-parametric model of the lidar system.

sented as a product of five independent dimensionless factors, each of them having its own nature.

The structure of a dimensionless-parametric model of the lidar presented in Fig. 3 shows the relationships between the normalised system parameters L_0, Φ_{ex}, Q, W, r and the measuring system components, including the state of the atmospheric object being sounded, lidar transmitter and receiver, interferences, reference medium, reference range and reference background brightness.

4.2. Results of dimensionless-parametric modelling of laser remote sensing of the atmosphere

Let us analyse how strong can be the impact of a bright background interference caused by the scattered radiation of the sky. According to the estimates (16), the background interference impact (just as that of the internal noise) on the lidar receiver sensitivity is not direct, but indirect, through the optical-physical parameters of the investigated medium. In other words, a positive feature of the dimensionless-parametric approach is that the background can be evaluated as 'strong' or 'weak' in relation to a particular lidar which is sensing a particular object of the ambient air. Consider Fig. 4, in which the dependences of the signal-to-noise ratio on the relative background brightness for different values of A_0 and Π are presented.

As seen from Fig. 4c, the noisy photodetectors ($A_0 \gg 1$) are significantly less sensitive to the background noise: the signal-to-noise ratio at their output is only reduced at very intense sky background. In contrast, the low-noise detectors ($A_0 \ll 1$) in a comparatively transparent atmosphere ($\Pi \ll 1$) noticeably lose their sensitivity at low levels of background noise (Fig. 4a). At the same time, it is seen that, in respect of the signal-to-noise ratio and sensitivity, the noisy receivers with large A_0 values are inferior to the receivers with low internal noise even at a very low background.

For comparison, we can estimate the reduction in sensitivity and signal-to-noise ratio at the lidar receiver output under the impact of background radiation with respect to their levels in case of reference brightness, using the relation:

$$\Phi_b^{SNR} = \frac{\rho(b_{rel})}{\rho(b_{rel}=1)} = \sqrt{\frac{\Pi + A_0}{\Pi + A_0 + (b_{rel}-1)/S_{b0}}}.$$

Let us rewrite Eqn (11) for the normalised lidar signal $P_s/P_{s0} = \Pi$ in the form

$$S_q N \Pi^2 - \rho^2 \Pi - \rho^2 A = 0. \qquad (24)$$

Then threshold sensitivity for a given signal-to-noise ratio ρ is

$$\Pi_{thr} = \frac{\rho^2}{2S_q N}\left(1 + \sqrt{1 + 4S_q A N/\rho^2}\right)$$

$$= \frac{\rho^2}{2L_0^2(A_0+1)N}\left[1 + \sqrt{1 + 4(L_0^2 N/\rho^2)(A_0+1)A}\right],$$

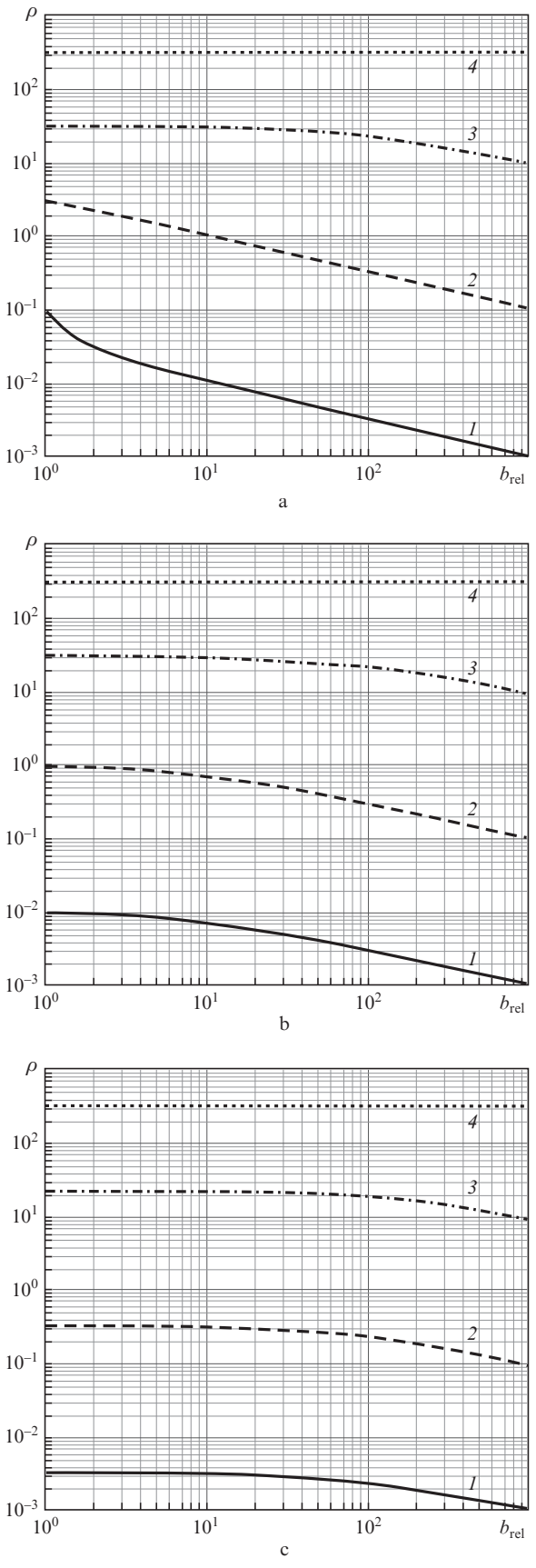

Figure 4. Signal-to-noise ratios as functions of the relative background interference level at $S_q = 100$, $\Pi = (1)\ 10^{-3}$, $(2)\ 10^{-1}$, $(3)\ 10$ and $(4)\ 10^3$ for $A_0 =$ (a) 10^{-2}, (b) 1 and (c) 10.

or

$$\Pi_{\text{thr}} = \frac{\rho^2}{2L_0^2(A_0+1)N} \times \left\{1 + \sqrt{1 + 4(L_0^2 N/\rho^2)(A_0+1)[A_0 + (b_{\text{rel}}-1)/S_{\text{b0}}]}\right\}. \quad (25)$$

For a comparatively transparent medium under study, when $W^2 \approx 1$ (i.e., a value of $W^2 > 0.9$ is achievable at $\alpha R < 0.05$), we can write (see Appendix 2) $\Pi \approx Qr^{-2}$, where $r \approx \sqrt{Q/\Pi}$. Therefore, the maximum operation range for a given signal-to-noise ratio ρ can be presented in the form

$$r_{\max} = \frac{L_0}{\rho}\left\{\frac{2(A_0+1)NQ}{1 + \sqrt{1 + 4(L_0^2 N/\rho^2)(A_0+1)[A_0 + (b_{\text{rel}}-1)/S_{\text{b0}}]}}\right\}^{1/2},$$

or

$$r_{\max} = \frac{\sqrt{S_q}}{\rho}\left\{\frac{2NQ}{1 + \sqrt{1 + 4(S_q N/\rho^2)[A_0 + (b_{\text{rel}}-1)/S_{\text{b0}}]}}\right\}^{1/2}.$$

4.3. Lidar range reduction under the impact of intense background radiation

The impact of background radiation on the lidar operation range for $N = 1$ and $\rho = 1$ can be estimated from the relation:

$$r_{\text{b}} = \frac{r_{\max}(b_{\text{rel}})}{r_{\max}(b_{\text{rel}}=1)} = \left[1 + \sqrt{1 + 4L_0^2 A_0(A_0+1)}\right]^{1/2} \times \left\{1 + \sqrt{1 + 4L_0^2(A_0+1)[A_0 + (b_{\text{rel}}-1)/S_{\text{b0}}]}\right\}^{-1/2}. \quad (26)$$

Different sensitivities of noisy and low-noisy receiving lidar systems to background radiation defined by $b_{\text{rel}} = B_\lambda/B_{0\lambda}$ are illustrated in Fig. 5. According to (26), noisy ($A_0 \geqslant S_{\text{b0}}^{-1}$) photodetectors ($A_0 = 10$) only react to a very strong sky background, while, at $A_0 \ll S_{\text{b0}}^{-1}$, low-noise photodetectors ($A_0 = 10^{-2}$) are sensitive to the comparatively low sky background levels.

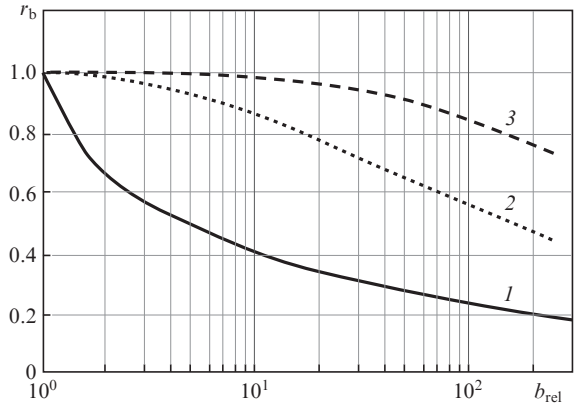

Figure 5. Lidar ranges as functions of the background radiation at $A_0 =$ $(1)\ 10^{-2}$, $(2)\ 1$ and $(3)\ 10$, $S_{\text{b0}} = 10$.

4.4. Dimensionless-parametric approach to evaluation of the lidar potential with PMT, APD, and Si-PMT as photodetectors

First and foremost, we should note that in modern lidar systems [5, 6, 8–20, 26–32, 34–39, 41] that are applied in the spectral range from the UV to near-IR range, the most sensitive and therefore the typical photodetectors are photomultipliers (PMT), avalanche photodiodes (APD) and solid state silicon photomultipliers (Si-PMT). As defined in (12), the dimensionless parameter A_0 characterises the impact of quantum and internal noise of the receiver, and also a minimal level of background noise. Consider the spectral changes A_0 as a measure of noise in a lidar receiver, which exceeds the quantum noise in the wavelength range of 0.3–1.1 μm.

Figure 6 shows the simulation results of the A_0 parameter behaviour, adapted to the spectral and energy characteristics of PMT, APD, and Si-PMT. Figure 6 also presents spectral dependences of an inverse value of the previously introduced partial ratio of the reference signal to the reference level of the background interference $S_{b0} = P_{s0}/P_{b0}$, which is independent of the type of photodetector.

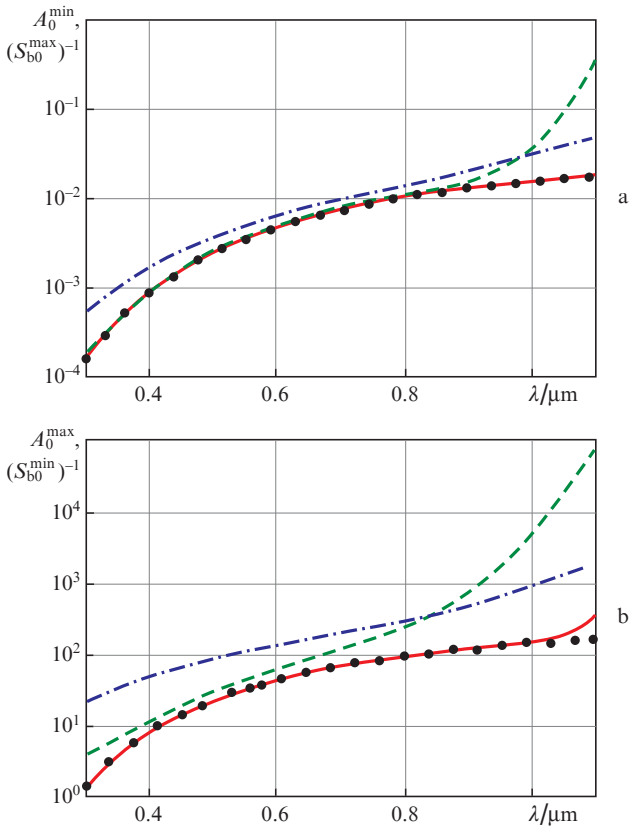

Figure 6. (Colour online) Spectral dependences of the parameter A_0 for PMT (solid curves), APD (dot-dashed curves), and Si-PMT (dashed curves), and also (a) the upper and (b) lower limits of the inverse partial ratio $S_{b0}^{-1} = P_{b0}/P_{s0}$ (points).

Comparison of the excess noise levels of three types of high-sensitivity photodetectors, the impact of which describes the parameter A_0, shows that the lower limit of A_0 (characterising the low-noise photodetectors) in virtually all cases is close to the constraint level defined by the minimum level of

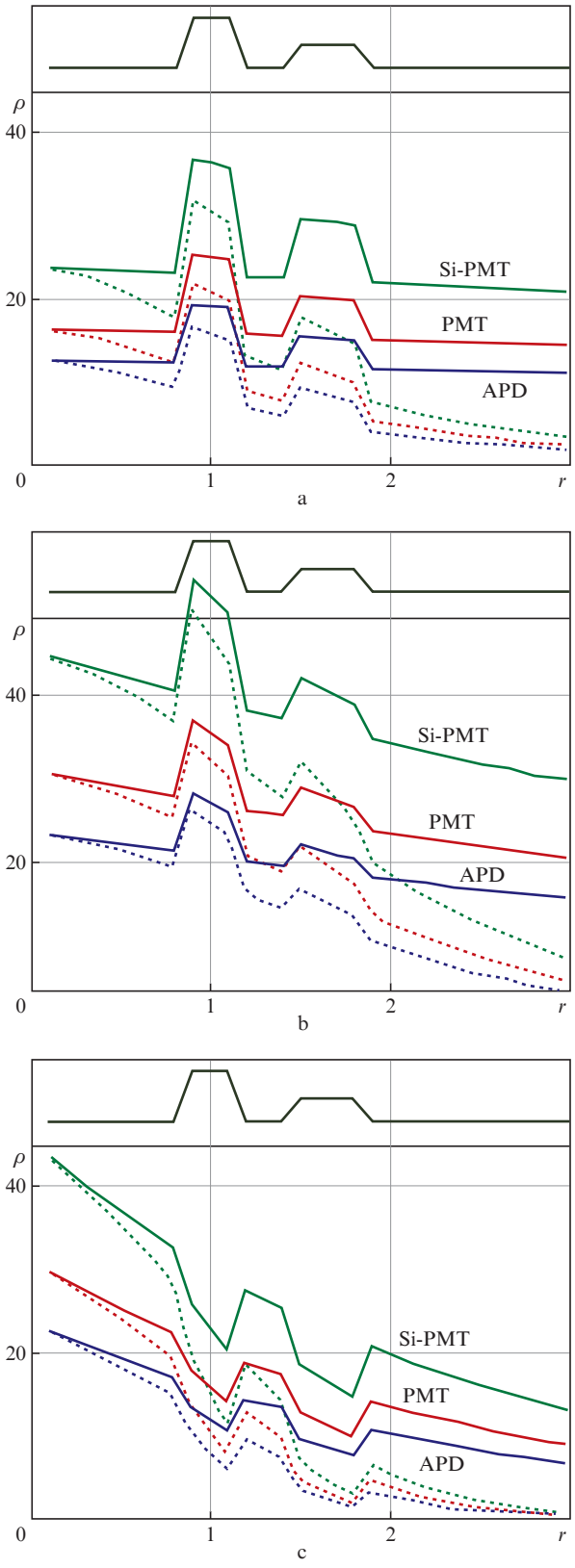

Figure 7. (Colour online) Range profile distortions of the signal-to-noise ratio, caused by background interference in the case of object sensing in the ambient atmosphere of different optical density for S_m = (a) 100, (b) 30 and (c) 10 km when using PMT as a photodetector (system parameter $L_0 = 10.9$; red curves), APD ($L_0 = 8.3$; blue curves), and Si-PMT ($L_0 = 15.9$; green curves). Solid curves show the reference background level ($b_{rel} = 1$), dashed curves – intensive background ($b_{rel} = 300$). Brown curves at the top of each Figure are the model profiles.

reference background noise. Given the variability of parameters of the commercially available models of PMT, APD and SI-PMT, we may note that the noisy PMT in the whole spectral range have a lower excess noise level than the other two types of receivers.

The combined impact of optical-physical parameters of the medium under study, background noise brightness and generalised parameters of the lidar transceiver on the measurement sensitivity and achievable signal-to-noise ratio is illustrated in Fig. 7. From a large series of results of model calculations, we have selected and shown several range profiles of the achieved signal-to-noise ratio, with a compensation for the range factor in sensing the model object (profiles in the upper part of Figs 7a–7c) in the ambient air of different optical density. When conducting model experiments at λ = 532 nm, the specifics of noise parameters of high-sensitive PMT, APD, and Si-PMT receivers have been taken into account.

Firstly, it is seen that, according to (11)–(13) and Fig. 4, the signal-to-noise ratio increases with decreasing meteorological visibility S_m. Secondly, the degree of signal attenuation on the path from the lidar to the object and back increases with increasing product αr (a decrease in the transparency along the sensing path), which, correspondingly, leads to a decrease in the signal and the signal-to-noise ratio. Finally, it is seen from Fig. 7 that, with an increase in Π factor, the impact of internal noise for different photodetectors is reduced (the ratio A_0/Π becomes much smaller than unity) and the range profiles of the signal-to-noise ratio become closer, thus reflecting only background interferences that are the same for all detectors.

4.5. Comparison of real lidar systems

Figure 8 shows the results of comparison of lidars A and B [36], basic parameters of which are given in Appendix 3. The dimensionless parameters of these lidars, calculated according to the above-proposed method, are given in Table 1. The generalised parameters L_{0A} and L_{0B} that predict the potential of lidars A and B in sensing the reference medium are defined at Π = 1. The values b_{rel} = 1, ~17 and 300 correspond to the simulation results for lidars A and B in atmospheric sensing with weak, average and bright sky background and with wide variations of its optical-physical parameters (parameter Π).

Table 1.

Lidar	S_q	S_n	S_{b0}	A_0	L_0
A	10^4	1.5×10^3	1.8×10^3	5×10^{-3}	98.4
B	4×10^2	4.3×10^4	3.5×10^4	3×10^{-5}	20.1

It follows from Figure 8 that lidar A has a greater potential compared to lidar B ($L_{0A} \approx 100$, $L_{0B} \approx 20$). It is seen that, under an intense sky background (for example, at b_{rel} = 300), lidar A is capable of receiving, with a given accuracy (for example, at ρ = 10), the echo-signals that are about 10 times weaker compared to lidar B. Thus, according to (26), the range r_b of lidar A under the impact of background brightness

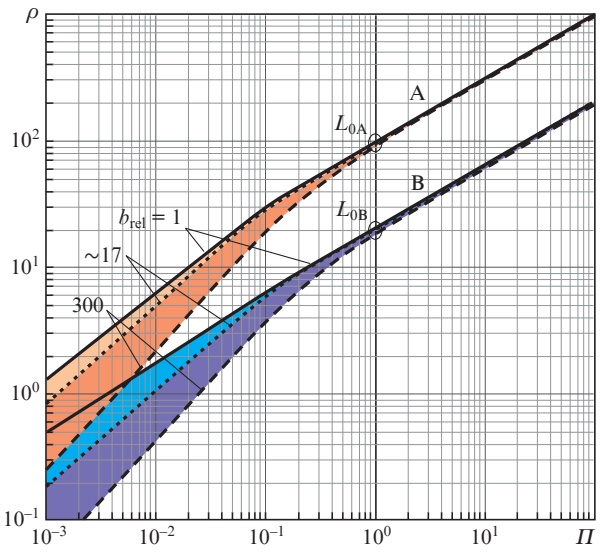

Figure 8. Dependences $\rho(\Pi)$ for lidars A and B sensing the same atmosphere at different levels of the ambient background interference b_{rel}.

with b_{rel} from 1 to 100 decreases from 1.00 to 0.55, while that of lidar B – from 1.00 to 0.77.

5. Conclusions

Based on the development and expansion of the methodology of dimensionless parameterisation, we have generalised characteristics of the laser systems for atmospheric sensing. The applied approach has allowed us to predict the characteristics of a wide variety of atmospheric backscatter lidars, from microlidars to power systems. The structure of a dimensionless-parametric model of the lidar system for atmospheric sensing is developed. The potentially feasible ranges of the signal-to-noise ratio and sensitivity of remote sensing systems under the conditions of wide variability of optical weather that allow the use of lidars are found: from the crystal-clear molecular atmosphere to fog, snow and rain. A variety of impact conditions of the daytime sky background interferences is analysed, which on a bright sunny day may severely limit the capability of lidar systems.

The fundamental difference between the proposed methodology and the traditionally accepted approaches is that the formation of several carefully justified dimensionless parameters based on the introduced reference parameters, and their subsequent use, allows one to reliably predict the most important potential characteristics of a particular lidar in specific conditions of the sensing path and sky background brightness. For example, it is possible to predict the variability of the signal-to-noise ratio at the photodetector output of a lidar system in sensing a selected part of the atmosphere in the range span being of interest to us, at a certain angle to the Sun that forms the background brightness under evaluation. Based on the proposed parameters and algorithms, it is also possible to predict the lidar system operation range.

Appendix 1. International visibility scale for different observation conditions

S_m/km	$T(R = 1$ km)	$\alpha(\lambda = 0.55$ μm)/km^{-1}	Observation conditions	Visibility characteristic
< 0.05	$< 10^{-34}$	> 78.24	Very strong fog	Very bad
0.05–0.20	3×10^{-9}–10^{-34}	19.56–78.24	Heavy fog, very thick snow	Bad
0.2–0.5	4×10^{-4}–3×10^{-9}	7.824–19.56	Moderate fog or heavy snow	
0.5–1.0	0.020–4×10^{-4}	3.912–7.824	Light fog, moderate snow, or strong haze	
1–2	0.141–0.020	1.956–3.912	Moderate snow, very heavy rain, or moderate haze	Medium
2–4	0.376–0.141	0.978–1.956	Light snow, heavy rain, or weak haze	
4–10	0.676–0.376	0.391–0.978	Moderate rain, very weak snow, or weak haze	Good
10–20	0.823–0.676	0.196–0.391	No rain or moderate rain	
20–50	0.823–0.925	0.078–0.196	Clean air with no rain	Very good
> 50	> 0.925	< 0.078	Absolutely clean air	Exceptional

Appendix 2. Ranges of parameters of the medium and sky background used in simulations

Meteorological visibility range S_m/km 0.1–100
Volumetric coefficient of scattering/attenuation of the atmosphere/km^{-1} 0.03–1.00
Sensing range R/km 0.1–30
Daytime sky background radiation brightness B_λ/W m^{-2} sr^{-1} m^{-1} . . . . . 10^6–3×10^8

Appendix 3. Typical parameter ranges of the atmospheric lidar used in simulations

		Lidar A	Lidar B
Laser radiation energy E/J	10^{-6}–1	0.15	0.13
Beam radiation divergence Θ/rad	10^{-3}–5×10^{-3}		
Beam radiation diameter d/mm	3–10		
Laser pulse duration τ_p/ns	10–100		
Pulse repetition rate f_{rep}/Hz	10–10^5	10	20
Receiving lens area A_D/m^2	10^{-2}–10^{-1}	0.03	0.09
Receiving telescope focal length F_t/m	0.5–1.5		
Optical receiving system transmittance ξ	0.05–0.50	0.50	0.08
Receiving telescope view field angle θ/rad	10^{-3}–3×10^{-3}	10^{-3}	1.5×10^{-3}
Optical filter bandwidth $\Delta\lambda$/nm	1–10	10	1
Receiving system bandwidth Δf/MHz	10–100	10	20
Lidar spatial resolution ΔR/m	3–30		
Quantum efficiency of typical photodetectors η	0.10–0.85	0.77	0.046
Photodetector noise factor F:			
PMT	1.2–1.5		1.5
APD	4–10	5.0	
Si-PMT	1.1–1.5		
Photodetector internal amplification factor M_d:			
PMT	3×10^5–3×10^6		
APD	40–200		
Si-PMT	10^6–4×10^6		
Photodetector dark current I_d/A:			
PMT	10^{-10}–10^{-9}		
APD	10^{-9}–10^{-8}		
Si-PMT	10^{-7}–10^{-6}		
Reduced noise-equivalent power (NEP) of the photodetector/W Hz$^{-1/2}$	$f(F,\Delta f,\lambda,\eta,I_d,M_d)$	3×10^{-14}	5×10^{-16}
Photodetector quantum noise power P_q/W	$f(F,\Delta f,\lambda,\eta)$	4.83×10^{-11}	4.86×10^{-10}
Photodetector internal noise power P_n/W	10^{-12}–10^{-9}	3×10^{-10}	5×10^{-12}
Reference range R_0/km	1		
Reference attenuation coefficient of molecular atmosphere α_0/km^{-1}	0.0116 ($\lambda = 0.55$ μm)		
Reference signal power P_{s0}/W	$f(E_0,A_D,\xi,\alpha_0,R_0,\lambda)$	4.72×10^{-7}	1.97×10^{-7}
Reference sky background radiation brightness $B_{0\lambda}$/W m^{-2} sr^{-1} m^{-1}	10^6		
Reference background noise power P_{b0}/W	$f(A_D,\xi,\Delta\lambda,\theta)$	2.65×10^{-10}	5.66×10^{-12}

References

1. Zuev V.E. *Laser-meteorolog* (Laser meteorologist) (Leningrad: Gidrometeoizdat, 1974) p. 184.
2. Hinkley D.E. (Ed.) *Laser Monitoring of the Atmosphere* (Berlin: Springer-Verlag, 1976) Vol. 14.
3. Measures R.M. *Laser Remote Sensing. Fundamentals and Applications* (New York: John Wiley & Sons, 1984; Moscow: Mir, 1987).
4. Bunkin A., Voliak K. *Laser Remote Sensing of the Ocean. Methods and Applications* (New York: Wiley & Sons, 2001).
5. Pershin S., Linkin V., Bukharin A., et al. *Proc. SPIE Int. Soc. Opt. Eng.*, **1752**, 293 (1992).
6. Moussavi M., Abdalati W. *Int. J. Remote Sens.*, **35** (13), 5263 (2014).
7. Bukharin A.V., Pershin S.M. *Opt. Atmos. Okeana*, **7** (4), 521 (1994).
8. Cao N., Zhou X., Li S., et al. *Rev. Sci. Instrum.*, **80** (3), 109 (2009).
9. Pershin S., Lyash A., Makarov V., et al. *Proc. SPIE Int. Soc. Opt. Eng.*, **7355**, 0S1 (2009).
10. Agishev R., Gross B., Moshary F., Gilerson A., et al. *Appl. Phys. B: Lasers Opt.*, **81** (5), 695 (2005).
11. Campbell J., Lin B., Nehrir A., et al. *Opt. Lett.*, **39** (24), 6981 (2014).
12. Papayannis A., Ancellet G., Pelon J., et al. *Appl. Opt.*, **29** (4), 467 (1990).
13. Veselovskii I., Whiteman D., Korenskiy M., et al. *Atmos. Chem. Phys.*, (15), 1647 (2015).
14. Osche G. *Optical Detection Theory for Laser Applications* (New York: Wiley, 2011).
15. Agishev R., Comeron A., Bach J., et al. *Opt. Laser Technol.*, **49**, 86 (2013).
16. Agishev R.R. *Lidarnyi monitoring atmosfery* (Lidar Monitoring of the Atmosphere) (Moscow: Fizmatlit, 2009).
17. Agishev R., Comeron A., Gilerson A. *Eur. Phys. J.: Laser Radar Ser.*, **119**, 2509 (2016).
18. Saleh B., Teich M. *Fundamentals of Photonics* (New York: Wiley, 2011).
19. Mona L., Arboledas A., Amiridis V., et al. *Eur. Phys. J.: Laser Radar Ser.*, **119**, 1902 (2016).
20. Pappalardo G., Amodeo A., Apituley A., Comeron A., et al. *Atmos. Meas. Tech.*, (7), 2389 (2014).
21. Ross M. *Laser Receivers* (New York–London–Sidney: John Wiley & Sons, Inc., 1966; Moscow: Mir, 1969).
22. Minkoff J. *Signal Processing Fundamentals and Applications for Communication and Sensing Systems* (Norwood: Artech House, 2002).
23. Ignatov A.N. *Optoelektronnye pribory i ustroistva* (Optoelectronic Devices and Equipment) (Moscow: Eco-Trends, 2006) p. 272.
24. Rosencher E., Vinter B. *Optoelectronics* (Cambridge: Cambridge University Press, 2002; Moscow: Technosphere, 2006).
25. Keiser G. *Optical Fiber Communications: Principles and Practice* (New York: McGraw-Hill, 2010).
26. Fukuchi T., Shiina T. *Industrial Applications of Laser Remote Sensing* (Sharjah: BenthamSci, 2012).
27. Kovalev V., Eichinger W. *Elastic Lidar: Theory, Practice, and Analysis Methods* (New York: Wiley-Interscience, 2004).
28. Agishev R., Gross B., Moshary F., Gilerson A., et al. *Opt. Lasers Eng.*, **44** (8), 779 (2006).
29. Agishev R., Gross B., Moshary F., Gilerson A., et al. *Appl. Phys. B: Lasers Opt.*, **80** (6), 765 (2005).
30. Agishev R., Comeron A., Gross B., Gilerson A., et al. *Appl. Phys. B: Lasers Opt.*, **79** (2), 255 (2004).
31. Krekov G.M., Matvienko G.G. *Atmos. Oceanic Opt.*, **23** (10), 835 (2010).
32. Molebny V., Kamerman G., Steinvall O. *Electron. Nanotechnol.*, (3), 185 (2011).
33. Privalov V.E., Fotiadi A.E., Shemanin V.G. *Lazery i ekologicheskii monitoring atmosfery* (Lasers and Environmental Monitoring of the Atmosphere (St. Petersburg: Lan', 2013).
34. Apituley A., Freudenthaler V., Comeron A., et al. *Proc. IEEE*, **2**, 414 (2008).
35. Agishev R., Comeron A., Rodriguez A., et al. *Appl. Opt.*, **53** (12), 3164 (2014).
36. Comeron A., Agishev R. *Proc. SPIE Int. Soc. Opt. Eng.*, **9242**, 1 (2014).
37. Rodriguez A., Rocadenbosch F., Sicard M., et al. *IOP Conferences Series: Earth and Environmental Science*, **28**, 13 (2015).
38. Rees W. *Physical Principles of Remote Sensing* (Cambridge: Cambridge University Press, 2012).
39. Weitkamp C. *Lidar: Range-Resolved Optical Remote Sensing of the Atmosphere* (Berlin: Springer, 2005).
40. Kaul' B.V. *Opt. Atmos. Okean.*, **2** (2), 211 (1989).
41. Donovan D., Whiteway J., Carswell A. *Appl. Opt.*, **32** (33), 6742 (1993).